A numerical study of correlations between wake meandering and loads within a wind farm

IOP Conf. Series: Journal of Physics: Conf. Series **1256** (2019) 012012 doi:10.1088/1742-6596/1256/1/012012

A numerical study of correlations between wake meandering and loads within a wind farm

Maud Moens[1], **Nicolas Coudou**[1,2,3], **Philippe Chatelain**[1]

[1] Institute of Mechanics, Materials and Civil Engineering, Université catholique de Louvain, Belgium
[2] Mechanical Engineering Department, Université de Mons, Belgium
[3] von Karman Institute for Fluid Dynamics, Belgium

E-mail: maud.moens@uclouvain.be

Abstract. This paper aims at the better understanding of the correlations between rotor loads and the wake meandering inside a wind farm. The flow rotor dynamics are simulated by means of Large Eddy Simulations coupled to Actuator Disk models. The wake meandering is captured through a centerline tracking, itself based on the available power in the flow. Two turbulence intensities are investigated, TIs = 6% and 10%. Results show that the yawing moment is very well correlated to the wake movement, even for wind turbines located deeper into the the wind farm. Correlations can also be found between the wake oscillation and the root bending moments. Wake signatures can also be identified from the amplitude of the high-frequency oscillations of the root bending moments; however, the correlation is sometimes less visible, and deviations can be correlated to wind events or wake decay.

1. Introduction

In a wind farm arrangement, turbines may be impacted by wakes of upstream machines. This leads to increased fatigue loads through the higher levels of turbulence within the wakes and the intermittency of the wake overlap due to meandering. A better understanding of the correlations between loads and wake meandering will allow their exploitations toward turbine-level load alleviation control and farm level collaborative schemes. The long-term objective consists in using blades as sensors to recover information about the incoming flow and using this information to control both individual turbines and wind farms.

This paper aims at tracking potential wake signatures from yawing and root bending moments. The correlations between the wake oscillation and the aerodynamic loads are already studied in several research papers [1],[2] but these mainly focused on finding the best predictor for the wake meandering downstream of the machine of interest. This study is centered more on the detection of a potential upstream wake impacting one rotor, based on the loads applied on that rotor. This work will also assess the level of the correlations between loads and upstream wake oscillation with respect to turbulence intensity or equivalently the position of the wind turbine into the wind farm.

We achieve this by performing unsteady wind farm simulations using Large Eddy Simulations coupled to an advanced Actuator Disk method [3]. This approach has the advantage to accurately capture the unsteady wake behavior and the rotor dynamics, while keeping acceptable computational costs, even for large wind farms. The wake centerline is tracked with a technique

based on the available power in the flow [4], which allows a straightforward comparison between the loads and the wake meandering.

The methodology for simulating the wind farms, for recovering root bending and yaw moments and for tracking the wake centerline is first presented in Section 2. Section 3 presents the set-up and the wind farm arrangement. Section 4 presents the results while our conclusions are drawn in Section 5.

2. Methodology

2.1. Flow solver

We consider the LES of incompressible turbulent flows. It is performed using a in-house developed fourth-order finite differences code [5], formulated in primitive variables (i.e. in velocity and pressure) and using a structured staggered mesh arrangement. The Navier-Stokes equations, supplemented by a subgrid scale (SGS) model, are solved using a fractional-step method [6] and are discretized in space using a fourth-order finite difference scheme. However, when a wall model is required, the first layer of off-wall points is computed with a second-order scheme (only in the wall normal direction) [7]. The Poisson equation for the pressure is solved using a multigrid solver with Gauss-Seidel smoother. The time integration is carried out using an explicit second-order Adams-Bashforth scheme. We use a classical Smagorinsky approach [8] for the SGS model. The wind turbine effect is added through external body forces (per volume) acting on the flow (discussed in Section 2.2). One wind farm simulation implies two concurrent simulations: this approach, as well as the boundary conditions are detailed in Section 2.3.

2.2. Actuator Disk model and recovering of fatigue loads

The chosen wind turbine model is a rotating Actuator Disk (AD) model, supplemented with a tip-loss correction [3]. The AD procedure implies a discretization in both radial and azimuthal directions, and the AD can non-uniformly react to wind fluctuations: this allows us to investigate loads on the rotor. These are recovered by replicating blade trajectories in the AD and by recomputing blade-attached quantities. The blade positions are computed based on an arbitrary initial position and the rotor speed history.

We here consider the blade root bending moments due to the aerodynamic forces and excluding gravity loading, i.e., the flapwise and edgewise moments. The flapwise moment, $M_{f,b}$, is caused by the force component aligned with the rotor axis and tends to bend the blades out of the rotor plane; the edgewise moment, $M_{e,b}$, is due to the tangential force component and contributes to the torque generation. They are evaluated for each blade as

$$M_{f,b} = \int_{R_{hub}}^{R_{tip}} (r - R_{hub})\, \mathbf{F_b}.\mathbf{e_n}\; dr \tag{1}$$

$$M_{e,b} = \int_{R_{hub}}^{R_{tip}} r\; \mathbf{F_b}.\mathbf{e}_\theta\; dr \tag{2}$$

where $\mathbf{F_b}$ is the aerodynamic force per length for the blade b; R_{hub} and R_{tip}, are the hub and the rotor radii; r is the radial position along the blade; $\mathbf{e_n}$ and $\mathbf{e}_\theta$, are the unit vectors in the normal and tangential directions to the rotor plane.

The yawing moment, denoted, M_z, is also investigated. This is caused by an imbalance in the forces with respect to the yaw axis, here the vertical axis at the hub location, $\mathbf{e_z}$. This can be expressed as:

$$M_z = \sum_{b=1}^{Nb} \mathbf{e_z}\; .\; \int_{R_{hub}}^{R_{tip}} \mathbf{x} \times \mathbf{F_b}\; dr \tag{3}$$

where Nb is the number of blades, and $\mathbf{x}$ is the vector position between the yaw axis and the considered force point. In this case, only the normal force component plays a role in the yaw moment, because the nacelle length is not taken into account; the distance between the rotor plane and the yaw axis is assumed to be zero.

The simulation tool is not coupled to an aeroelastic code, the blades thus act as rigid bodies. The wind turbine type is the "NREL offshore 5-MW baseline wind turbine" [9] and is improved with control schemes (torque and collective blade pitch controllers [9] and a yaw controller [10]).

As we only use an AD for the wind turbine model, without modeling the mast and the nacelle, we can only represent the wake meandering caused by the large scales of the atmospheric flow impacting the wind turbine and around the wake. The other potential sources of near and far wake oscillations, such as the instabilities of the tip and root vortices [11][12] or the presence of the nacelle [13], cannot be captured here.

2.3. Turbulence generation and wind farm simulation

One wind farm simulation implies two concurrent simulations. The main one actually involves the wind turbines, while the auxiliary one is used for generating inflow conditions (the domain size is the same for the two simulations).

For the auxiliary simulation, periodic conditions are enforced in the horizontal directions, while a no-through flow is imposed at the top. At the bottom, a wall stress model [7] for a rough wall is applied, to compute the surface shear stress as a function of the LES velocity field at the third vertical grid point and a roughness length, z_0. The flow is driven by an imposed pressure gradient, proportional to the friction velocity, u_τ and the height of the boundary layer, H : $\frac{1}{\rho}\frac{\partial p}{\partial x} = \frac{u_\tau^2}{H}$. z_0 and u_τ are determined so as to reach the desired hub velocity and level of turbulence.

This auxiliary simulation runs concurrently with the main simulation, which allows inflow conditions to be directly transferred to the inlet of the main domain. For the main simulation, outflow conditions are then imposed at the outlet boundary, while periodic conditions are kept in the spanwise direction. Again, a wall model and a no-through flow condition are imposed at the bottom and top, respectively.

In the present work, thermal and stratification effects are not included; the resulting simulations are thus equivalent to truly neutral atmospheric boundary layer cases.

2.4. Wake centerline tracking

We choose the most robust technique of Coudou et al. [4] to perform tracking of the wake centroid, (y_c, z_c), in cross-flow planes located downstream of a wind turbine (in the present work, x is the streamwise direction, y , the spanwise direction and z, the vertical direction). It is based on finding the minimum of a convolution product

$$(y_c, z_c) = \operatorname{argmin}\left(p\left(y, z\right) * f_G\left(y, z\right)\right) \tag{4}$$

between the available power density in the flow

$$p(y, z) = \frac{1}{2} u_x |\mathbf{u}|^2 \tag{5}$$

and a Gaussian masking function

$$f_G(y, z) = A \exp\left(-\left(\frac{(y-\mu_y)^2}{2\sigma_y^2} + \frac{(z-\mu_z)^2}{2\sigma_z^2}\right)\right) \tag{6}$$

with $A = 1$, $\mu_{y,z}$ is equal to the wind turbine center, and $\sigma_{y,z} = 0.5D$. Physically, this convolution method relies on the computation of the wind power inside a disk (with a Gaussian weighting)

located in a cross-flow plane and with a diameter equal to the rotor diameter D. This disk center position can be shifted in the $y-$ and $z-$directions; the wake center corresponds to the disk position for which the available power is minimum [14].

Finally, by tracking the wake centroid in several downwind cross-flow planes, the wake centerline can be obtained. For the wind farm simulations, the time-averaged velocity profile is substracted from the velocity field before computing the convolution.

3. Set-up

We here consider a wind farm with 15 machines. The domain size is $56D \times 32\text{D} \times 8\text{D}$ (D = 126 m, the diameter of the NREL-5WM [9]), with a grid of $N_x \times N_y \times N_z = 896 \times 512 \times 128$. The mesh is uniform in the horizontal directions, with a resolution of 16 points per D and $\Delta x = \Delta y = 7.875$ m. The grid is partially stretched in the vertical direction: the grid is uniform below 200 m with $\Delta z = 3.975$ m (i.e. 32 points per D) and above that, Δz increases to reach $\Delta z_{max} \simeq 23$ m at the top of the domain. This stretching and the used resolution prevent an AD force mollification at the lower point from affecting a sample location of the wall model. The time step is imposed to 0.125 s.

The wind farm arrangement consists in a array of three lines of five wind turbines, separated by 7D (see Fig. 1 for the locations of the 15 rotors). The first wind turbines are located at 12D from the inlet ($x/D = 0$ corresponds to streamwise position of the first row) and the first line is located at 9D from the lateral boundary ($y/D = 0$ is at the lateral boundary) (see Fig. 1).

Two turbulent intensities (TIs) are considered, 6 and 10 %, with a same hub velocity, $\bar{U}_{hub}$, of about 8 m/s. The TI is computed at hub height, based on the 3 velocity components: TI $= \sqrt{2/3k}/\bar{U}_{hub}$, where k is the turbulent kinetic energy. For TI = 6%, this corresponds to $u_\tau =$ 0.27 m/s and $z_0 \simeq 0.001$ m; for TI = 10%, $u_\tau = 0.44$ m/s and $z_0 \simeq 0.09$ m.

The wake meandering tracking has been performed in a post-processing step. The three-dimensional velocity field has been saved every 2 seconds for a period of 882 s, corresponding to $T = 56D/U_{hub}$ (the storage starts after $2T$), and the wake centerline positions are tracked over this period. The loads are computed on the same period, based on the recovered disk forces saved at every time step of the simulation (each 0.125 s).

4. Results

We mainly focus our analysis on the horizontal wake movement, which is more important than the vertical movement, and thus strongly influences the variations of the loads on the wind turbines.

4.1. Wake meandering

We first compare the wake movement for the two TIs. Figure 1 shows horizontal planes of instantaneous streamwise velocities at hub height, for the two TIs; the wake centerline positions are also reported on Fig. 1. For TI = 6% (Fig. 1(a)), as expected, the ambient wind fluctuations are weaker that those observed for TI = 10% (Fig. 1(b)). The wakes are also globally more structured, and are still well marked deeper in the wind farm. For TI = 10%, the wakes are sometimes rapidly deconstructed downstream of the wind turbine and their centerline are thus more difficult to track.

For both TIs, the wake movement increases for the downstream machines. This is better highlighted with the dimensionless horizontal wake movement, presented as a function of time and axial location in Fig. 2, for the three lines of wind turbines. For this wind farm configuration, the algorithm only seeks one minimum per line; the amplitude thus always goes to zero at the rotor position (vertical white areas at the rotor positions). For the lowest TI, the averaged wake centerline position is centered more around $y_c - y_{Li}/D$, where y_{Li} is the spanwise position of the line Li. For TI = 10%, the wake centerline is centered at $y_c - y_{Li}/D > 0$ or < 0 for relatively long

periods; we also notice additional higher frequency oscillations around these centers. The integral length scale of the transverse velocity fluctuations (computed in the precursor simulation) is very similar for both TIs: this does not explain the low frequencies of the wake oscillation observed in that case. The wake meandering is a quite complex process, which supposedly results from a combination of several phenomena: the size of the freestream flow structures, the energy content of those structures but also the interactions between the flow and the wind turbine. This should be investigated in more details to explain the low frequency oscillations.

It is planned to use a predictive method based on the estimation of the wake advection to determine the region where the minimum/minima should be located. This new approach should smooth the signal and avoid jumps in the wake centerline position, such as those noticeable in Figs. 1(a) and 1(b), around $x/D = 50$.

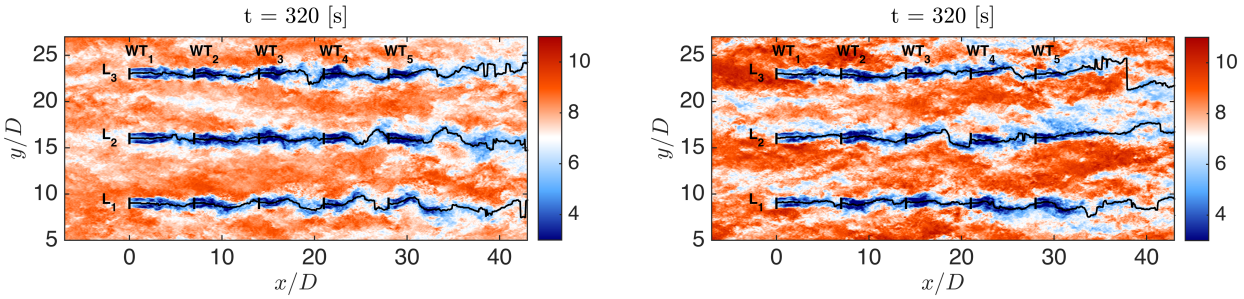

(a) TI = 6% (b) TI = 10%

Figure 1: Snapshots of the axial velocity in a horizontal plane located at hub height, with the wake centerlines (solid black lines). Left, TI = 6%, and right, TI = 10%. The units are in [m s$^-$1].

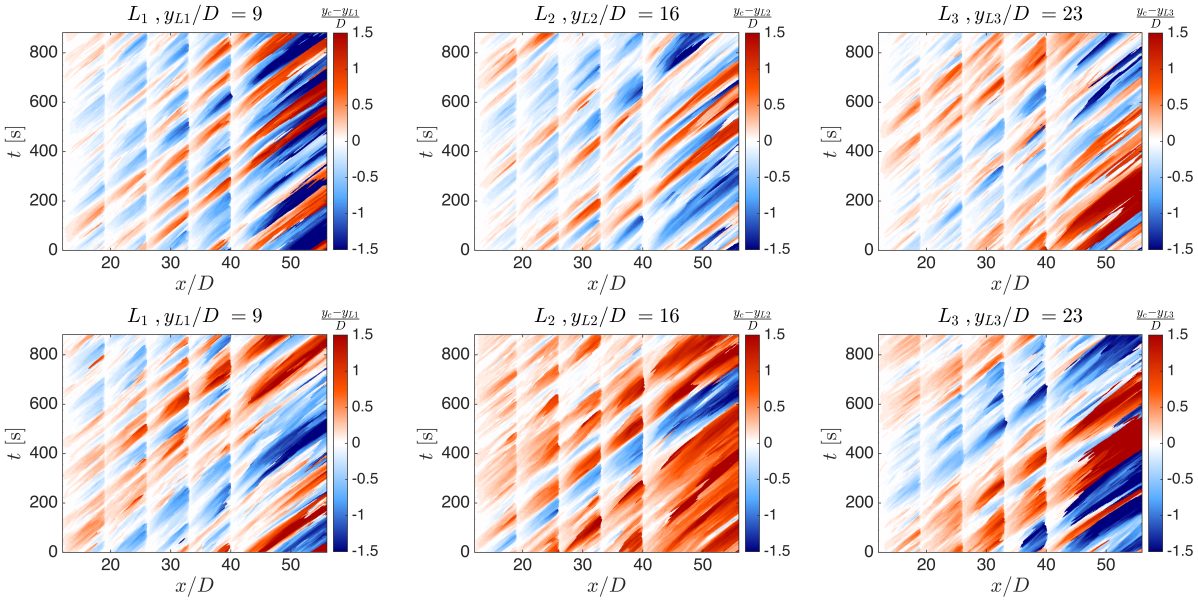

Figure 2: Dimensionless horizontal wake movement for the three lines of wind turbines, as a function of the time, t, and the adimensional axial position, x/D. Top, TI = 6%, and bottom, TI = 10%.

4.2. Comparison between loads and wake meandering

In this section, we compare (for both TIs) the wake centerline movement at a location of less than 0.5 D in front of one wind turbine WTi and the resulting moments on this rotor. We here consider two wind turbines, WT2 and WT5, respectively the second and the last rotors of the line L_3 (see Fig. 1(a) for the locations of these rotors). This aims at comparing the evolution of correlations between loads and wake meandering according to the depth of the wind turbine into the wind farm. In the following figures, Y_{wm} corresponds to $y_c - y_{wt,i}$, where $y_{wt,i}$ is the spanwise location of the wind turbine WTi.

4.2.1. Filtered yawing and root bending moments In this investigation, the yawing and the root bending moments are filtered in order to remove the high frequency oscillations due to the blade rotation; they are denoted M_z^f, $M_{f,b}^f$ and $M_{e,b}^f$. This allows to highlight the large scale fluctuations that can be potentially attributed to the wake meandering.

Figure 3 compares the yaw moment on a wind turbine WTi and the horizontal wake meandering just in front of this rotor. For WT2 (see Figs. 3(a) and 3(b)), the yaw moment is very well correlated with the horizontal wake movement, and this for both TIs. For the wind turbine located deeper in the wind farm (see Figs. 3(c) and 3(d)), the link is still visible, although slightly less marked than for WT2. The high-frequency oscillation of the wake meandering around $t = 500$ s is due to the chosen technique for tracking the wake position; this will be better explained and highlighted in Section 4.2.2.

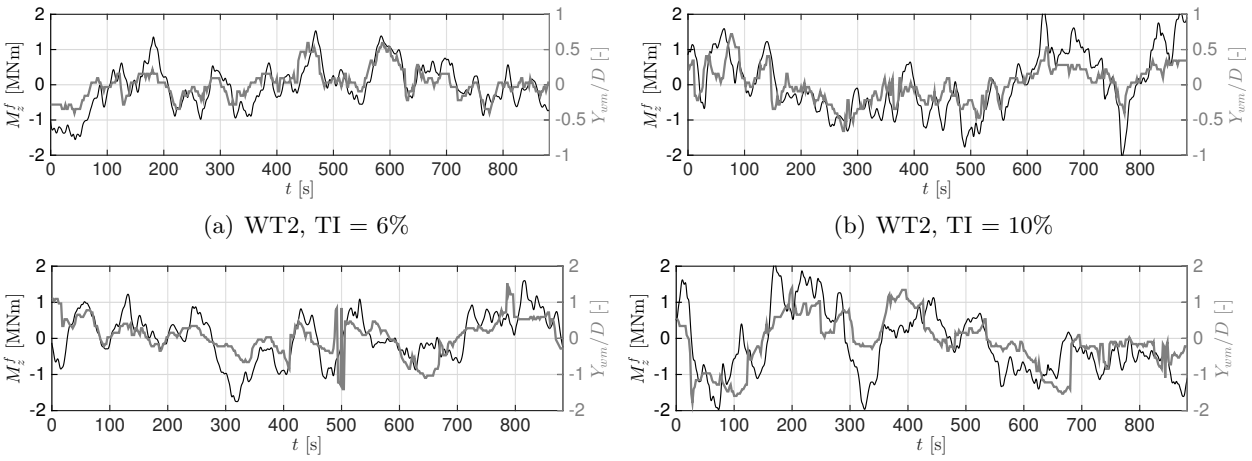

(a) WT2, TI = 6%

(b) WT2, TI = 10%

(c) WT5, TI = 6%

(d) WT5, TI = 10%

Figure 3: Comparison between the wake centerline position just upstream of WTi (solid grey line) and the resulting filtered yaw moment on WTi (solid black line). Two wind turbines are studied, WT2 (top) and WT5 (bottom), for the two TIs (left : 6% and right, 10%)

The normalized cross-correlations between the filtered yaw moment and the horizontal wake movement are presented in Fig. 4. They are computed based on:

$$R_{M_z^f Z_{wm}}(x,\tau) = \frac{\overline{M_z^f(t)\, Z_{wm}(x,t+\tau)}}{\overline{M_z^f(t)^2}\;\overline{Z_{wm}(x,t)^2}} \tag{7}$$

The correlations are investigated with the wake meandering signal just upstream of WT2 and WT5, but also at several locations downstream of those machines. The idea is to verify if the cross-correlation remains high enough downstream of the machine to consider using the yaw moment as a predictor for the wake meandering and feeding in a wake model. This study is

similar to the one Muller et al.[1] performed experimentally for one or two wind turbines; they highlighted the correlation between the yaw moment and the wake meandering when the wind turbine was disturbed by an incoming wake. In [2], the authors also concluded that the forces (the lateral force in that case) should not be neglected for predicting the downstream wake oscillation. We here verify the correlation in a line with more than two machines.

Globally, for WT2 and both TIs, the cross-correlation is higher than 0.75 when the upstream wake meandering signal is used. For WT5 and both TIs, it is slightly less important, as already noticed in Fig. 3. For locations further downstream from WT2, the cross-correlations remain high for TI = 6%, while they are more degraded for TI = 10%. This can be explained by the higher level of ambient turbulence, which distorts more the flow structures during the advection process. For WT5 and TI = 6%, the cross-correlation is really degraded for downstream locations, and drops to about 0.25 at 5D downstream of the rotor. On the contrary, it remains high for the case TI = 10%. To really explain this difference, the flow downstream of WT5 should be investigated in more details for both TIs. We leave this as a subject for further investigations as it is not the main subject of this paper.

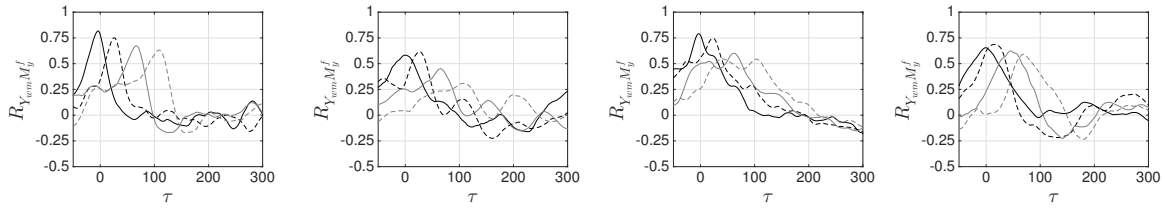

(a) WT2, TI = 6% (b) WT5, TI = 6% (c) WT2, TI = 10% (d) WT5, TI = 10%

Figure 4: Normalized cross-correlations between the horizontal wake movement and the filtered yaw moment on WTi, at x_i/D = -0.35 (solid black line), 1 (dashed black line), 3 (solid gray line), and 5 (dashed gray line) (x_i/D is relative to WTi). Two wind turbines are studied, WT2 and WT5, for the two TIs (left : 6 % and right, 10 %)

In Fig. 5, we compare the root bending moments for the blade $b = 1$ of the wind turbine WTi and the absolute horizontal wake centerline position, $|Y_{wm}|$, just in front of WTi. Again, the large scale oscillations can be linked to the wake movement. Indeed, when the wake is well centered in front of the rotor, the blades encounter low velocities everywhere on the rotor, leading to lower forces and so, lower root bending moment. When the wake partially immerses the rotor, on one rotation, the blades are also subjected to higher velocities in the wake-free area. The forces and, thus, the resulting root bending moments are globally higher.

4.2.2. Magnitude Analysis When we consider the unfiltered root bending moments (see example in Fig. 6, for the flapwise moment of WT2 and TI = 6%), we see that the amplitude of the high frequency-fluctuations varies according to the time. In the example shown in Fig. 6, around the time $t = 550s$, the amplitude is higher than around $t = 450s$ or $t = 600s$. This seems to corresponds to periods where the wind turbine is partially or fully immersed in the upstream wake. When the rotor is partially immersed, as explained in Section 4.2.1, the blade crosses the low velocities of the wake and the high velocities of the freestream flow. Over a period of one blade rotation, the amplitude of fluctuations is thus higher than that for periods where the usptream wake fully immerses the rotor. A potential wake signature may thus be recovered from an analysis of these magnitude variations.

We thus compute the power spectra of the root bending moments over a moving time period corresponding to about five blade rotations, and we save the magnitude of the spectra at the

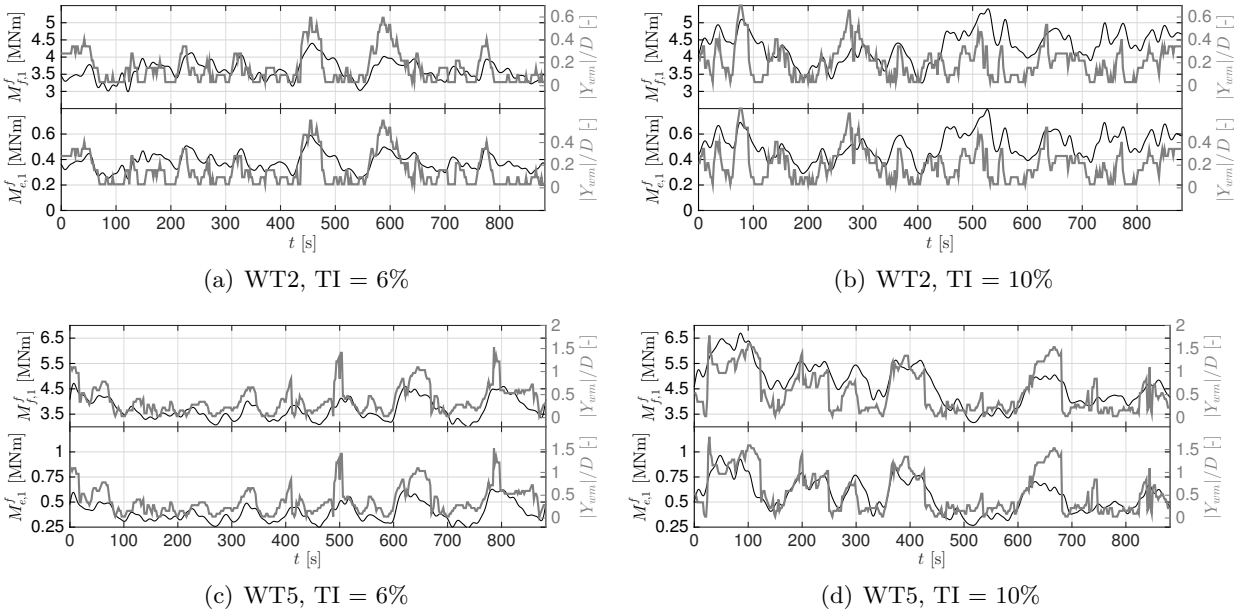

(a) WT2, TI = 6%

(b) WT2, TI = 10%

(c) WT5, TI = 6%

(d) WT5, TI = 10%

Figure 5: Comparison between the wake centerline position just upstream of WTi (solid grey line) and the resulting filtered flapwise and edgewise moments for the blade one of WTi (solid black line). Two wind turbines are studied, WT2 (top) and WT5 (bottom), for the two TIs (left : 6 % and right, 10 %).

blade rotation frequency, f_{rot}. The resulting signals $|MF_{f_{rot}}|$ and $|ME_{f_{rot}}|$ are reproduced in Fig. 7 and compared to the absolute value of the horizontal wake centerline position.

For TI = 6% and for WT2, the variation of the amplitude is globally correlated to the wake movement. For the case TI = 10% and the same wind turbine, the correlation is less marked from $t = 350s$; the amplitude oscillates in the same way as the wake centerline but the jump in magnitude observed at time $t = 350s$ appears to be uncorrelated to the wake movement. This is explained by a change of the ambient wind conditions around WT2; this is highlighted in Fig. 8(b) where instantaneous velocities around the third line are shown for several times for the case TI = 10%. We see that for $t = 100s$, and $t = 320s$ the incoming wind is slower, with areas of low velocities around the second wind turbine. Even if the rotor is partially immersed in the upstream wake, the blade crosses a freestream flow with lulls and the contrast with the wake is relatively weak. On the contrary, around $t = 450s$, the wind velocity around WT2 is globally higher, and the contrast with the wake is more important, increasing the amplitude of the high-frequency oscillations of the root bending moments. It is not shown in the paper, as we could only include a limited number of snapshots, but this situation of higher wind speed begins around $t = 350s$, and remains until a time of about $800s$; this is thus correlated with the increase in amplitude observed in Fig. 7(b).

For the wind turbine located deeper in the wind farm, the correlations are less marked. For example, for TI = 10% (see Fig. 7(d)), we see that the magnitude drops around $t = 100$s, while the wake position is strongly decentered. In fact, the rotor is totally out of the wake (see Fig. 8(b)) and the magnitude of the high-frequency oscillations of the root bending moments decreases. This behavior is thus still related to the wake meandering, even if it not visible at first sight on Fig. 7(d). This also explains the deviation observed around $t = 400$s for TI = 10% (the snapshot of velocities is not shown here), or around $t = 650$s for TI = 6% (see Figs 7(c) and 8(a)).

For the highest TI, around $t = 320$ s, the magnitude increases, while the wake remains

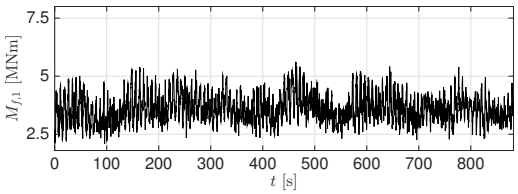

Figure 6: Flapwise moment for blade one of WT2, for the case TI = 6%.

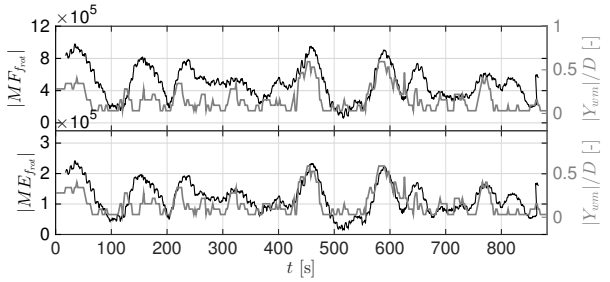

(a) WT2, TI = 6%

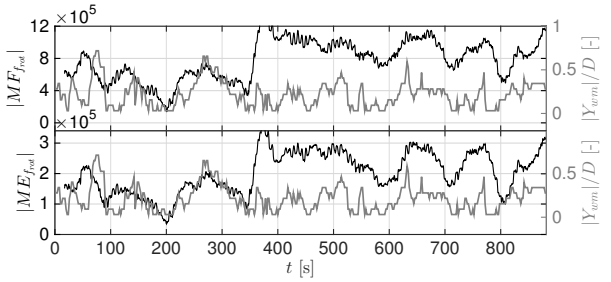

(b) WT2, TI = 10%

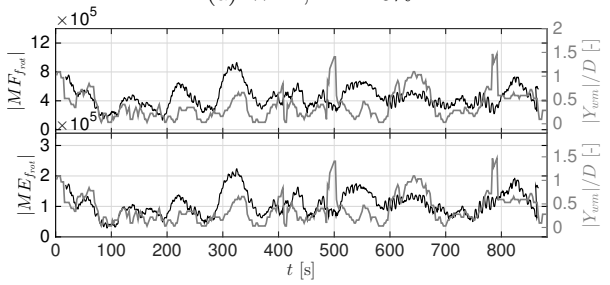

(c) WT5, TI = 6%

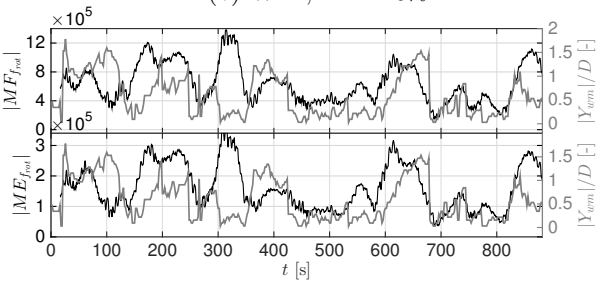

(d) WT5, TI = 10%

Figure 7: Comparison between the wake centerline position just upstream of WTi (solid grey line) and the amplitude at f_{rot} of the one blade flapwise and the edgewise moments for one blade. Two wind turbines are studied, WT2 (top) and WT5 (bottom), for the two TIs (left: 6% and right: 10%).

centered around the wind turbine location. In Fig. 8(b), at $t = 320$ s, we see the wake in front of the WT5 is deconstructed and is narrower than the rotor diameter. So, even if the wake is centered, the blade crosses the high velocities of the freestream flow and the low velocities of the wake, increasing the amplitude of the root bending moment oscillations.

A last remark for TI = 6% concerns the strong change in the wake center location around $t = 500$s for WT5 (as already mentioned in Section 4.2.1). With the current algorithm, we only seek one minimum per line. However, around $t = 500$s, in addition to the wake, there are some regions with low velocities (see 8(a), just in front of WT5). They are due to the remaining of other upstream wakes, and the minimum available power detected by the algorithm does not correspond to the wake of the fourth machine but rather to the wake remnant of the third one. This wake has not completely merged with the following one while being advected by the flow. This artificially increases the oscillation. This situation also happens around t=800s (the snapshot of the velocities is not shown here). The deviations are thus due to the tracking algorithm, and an improvement of the technique (as mentioned in Section 4.1) could decrease these artificial oscillations.

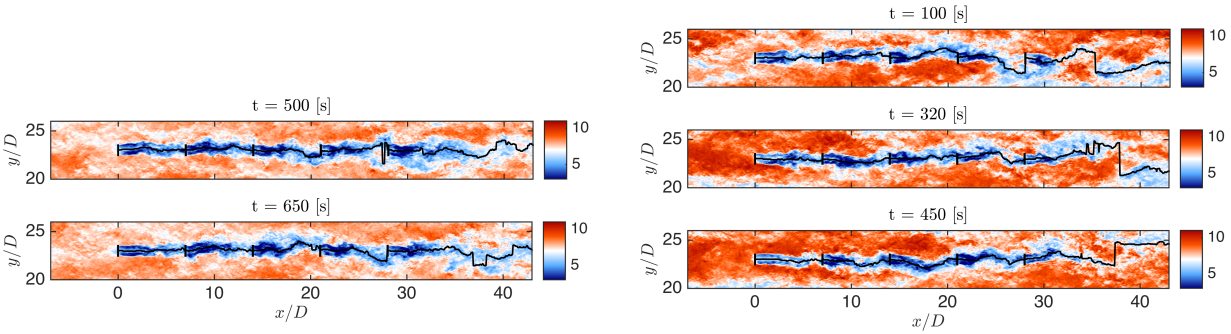

(a) TI = 6% (b) TI = 10%

Figure 8: Snapshots of the axial velocity in a horizontal plane located at hub height, centered around the line L_3, for the two TIs. The units are in [m s^{-}1].

5. Conclusions and perspectives

In this work, we investigated correlations between loads and the wake meandering for wind turbines in a wind farm arrangement. We performed Large Eddy Simulations, coupled to an advanced Actuator Disk (AD) model, which allowed to accurately capture the unsteady wake behavior and the rotor dynamics. The loads were recovered by replicating blade trajectories in the AD and by recomputing blade-attached quantities. The wake centerline position was tracked using an approach based on the available power in the flow.

Two turbulence intensities were investigated, TI = 6% and TI = 10%, and the loads were analyzed for two wind turbines, located at the beginning and deep in the wind farm, respectively. The yawing moments were well correlated with the wake oscillations upstream of rotors. The correlations were slightly less marked for rotors located deeper in the wind farm or for the highest TI, but the wake signature was clearly visible in all cases. We rapidly investigated the cross-correlation between the yawing moment and the wake meandering signal at the several locations (upstream and downstream of the machine of interest). The cross-correlations were globally high for all cases when the wake meandering just upstream of the rotor is used, even if they slightly decreased for wind turbines located deeper into the wind farm. The correlation between the yaw moment and the wake oscillation at downstream locations remained globally visible, but the cross-correlation dropped in certain cases. This analysis should be linked to the flow, to explain this important decrease in some cases. Filtered edgewise and flapwise moments were also linked to the upstream horizontal wake movement, but the correlations were slightly less noticeable than those obtained with the yawing moments. A final analysis was performed by investigating the amplitude of the high-frequency oscillations of the root bending moments. Again, a wake signature was found although we noticed some discrepancies: the variation of the amplitude could not always be linked to the wake movement and may be due to wind events, wake decay or merging with wakes of the rotors located further upstream in the wind farm.

These preliminary results show that wake meandering can be tracked from the loads, and are promising for the use of the blade data as sensors for future wind turbine or wind farm control. However, improvements could be brought. First, we could couple the wind farm simulation to an aeroelastic code, in order to obtain a more realistic response of the blade in terms of loads. Second, the wake tracking algorithm could clearly benefit from simple, and already identified, developments in terms of predictive smoothing and data structure strategies. It should then be able to handle complex wake interaction events and estimate wake widths within farms. Third, we here consider a small wind farm, with one fixed spacing. Further investigations could be performed by considering wind farms with more rotors or several wind turbine spacings or arrangements. Finally, this work could be extended to investigate in more details the link

between the loads and the wake meandering downstream of the turbine.

Acknowledgments
This project has received funding from the European Research Council (ERC) under the European Unions Horizon2020 research and innovation program (grant agreement no. 725627). The simulations used computational ressources made available on the Tier-1 supercomputer of the Fédération Wallonie-Bruxelles, infractructures funded by the Walloon Region under the Grant Agreement no. 1117545.

References

[1] Muller Y A, Aubrun S and Masson C 2015 Experiments in Fluids **56** 53 ISSN 1432-1114 URL https://doi.org/10.1007/s00348-015-1923-9
[2] Aubrun S, Muller Y A and Masson C 2015 Journal of Physics: Conference Series **625** 012005
[3] Moens M, Duponcheel M, Winckelmans G and Chatelain P 2018 Wind Energy
[4] Coudou N, Moens M, Marichal Y, Van Beeck J, Bricteux L and Chatelain P accepted Journal of Physics: Conference Series (proceedings of Torque 2018) (IOP Publishing)
[5] Duponcheel M, Bricteux L, Manconi M, Winckelmans G and Bartosiewicz Y 2014 International Journal of Heat and Mass Transfer **75** 470–482 ISSN 0017-9310
[6] Lee M, Oh B and Kim Y 2001 Journal of Computational Physics **168** 73–100 ISSN 0021-9991
[7] Thiry O 2017 Direct and large-eddy simulation of turbulent wall-bounded flows Ph.D. thesis École polytechnique de Louvain-Universitćatholique de Louvain
[8] Smagorinsky J Monthly Weather Review **91** 99–164
[9] Jonkman J, Butterfield S, Musial W and Scott G 2009 Definition of a 5-MW Reference Wind Turbine for Offshore System Development Tech. Rep. TP-500-38060 NREL
[10] Kooijman H J T, Lindeburg C, Winkelaar D and van der Hooft E 2003 Dowec 6 MW Pre-design: Aero-elastic modeling of the DOWEC 6 MW pre-design in PHATAS Tech. rep. DOWEC Dutch Offshore Wind Energy Converter 1997-2003 Public Reports Petten, the Netherlands
[11] Chamorro L P, Hill C, Morton S, Ellis C, Arndt R E A and Sotiropoulos F 2013 Journal of Fluid Mechanics **716** 658670
[12] Okulov V, Naumov I, Mikkelsen R, Kabardin I and Srensen J 2014 Journal of Fluid Mechanics **747** 369380
[13] Foti D, Yang X, Campagnolo F, Maniaci D and Sotiropoulos F 2018 Physical Review Fluids **3** 054607 (*Preprint* 1802.03836)
[14] Vollmer L, Steinfeld G, Heinemann D and Kühn M 2016 Wind Energy Science **1** 129–141